Macromolecular Research

Volume 16, Number 7 October 31, 2008

Review

Small-Angle X-ray Scattering Station 4C2 BL of Pohang Accelerator Laboratory for Advance in Korean Polymer Science

Jinhwan Yoon, Kwang-Woo Kim*, Jehan Kim, Kyuyoung Heo, Kyeong Sik Jin, Sangwoo Jin, Tae Joo Shin, Byeongdu Lee, Yecheol Rho, Byungcheol Ahn, and Moonhor Ree*

Pohang Accelerator Laboratory, Dept. of Chemistry, National Lab for Polymer Synthesis & Physics, Center for Integrated Molecular Systems, and Polymer Research Institute, Pohang University of Science and Technology, Pohang 790-784, Korea

Received June 28, 2008; Revised July 13, 2008; Accepted July 15, 2008

Abstract: There are two beamlines (BLs), 4C1 and 4C2, at the Pohang Accelerator Laboratory that are dedicated to small angle X-ray scattering (SAXS). The 4C1 BL was constructed in early 2000 and is open to public users, including both domestic and foreign researchers. In 2003, construction of the second SAXS BL, 4C2, was complete and commissioning and user support were started. The 4C2 BL uses the same bending magnet as its light source as the 4C1 BL. The 4C1 BL uses a synthetic double multilayer monochromator, whereas the 4C2 BL uses a Si(111) double crystal monochromator for both small angle and wide angle X-ray scattering. In the 4C2 BL, the collimating mirror is positioned behind the monochromator in order to enhance the beam flux and energy resolution. A toroidal focusing mirror is positioned in front of the monochromator to increase the beam flux and eliminate higher harmonics. The 4C2 BL also contains a digital cooled charge coupled detector, which has a wide dynamic range and good sensitivity to weak scattering, thereby making it suitable for a range of SAXS and wide angle X-ray scattering experiments. The general performance of the 4C2 BL was initially tested using standard samples and further confirmed by the experience of users during three years of operation. In addition, several grazing incidence X-ray scattering measurements were carried out at the 4C2 BL.

Keywords: small-angle X-ray scattering, wide-angle X-ray scattering, *in-situ* X-ray scattering, transmission X-ray scattering, grazing-incidence X-ray scattering, synchrotron radiation sources, Pohang Accelerator Laboratory, beamline, detector, polymers.

Introduction

Wide and small angle X-ray scattering (WAXS and SAXS) are the principal tools of the structural analysis of polymers, fibers, metals and alloys, liquid crystals, and colloidal systems.[1-44] These techniques provide information such as the shape and size of macromolecules, the characteristic distances of partially ordered materials, and pore sizes. The use of synchrotron sources with not only a high photon flux but also low beam divergence can greatly expand the range of applications of WAXS and SAXS techniques, such as in

*Corresponding Authors. E-mails: ree@postech.edu or xraykim@postech.ac.kr

time-resolved measurements of bulk samples and thin films with nanoscale thickness.[45-63]

The 4C1 beamline (BL)[64] at the Pohang Accelerator Laboratory (PAL)[65] was the first dedicated synchrotron small-angle X-ray scattering station in Korea.[45-53,66-73] This BL is based on a bending magnet and was designed for time-resolved studies of polymer and fibrous materials. The optical component of the 4C1 BL consists of a double multilayer monochromator (DMM) and a focusing mirror. The 4C1 BL has been used to elucidate polymer structure and morphology by the polymer research groups of Korea.

To satisfy the rapid growth in the SAXS requirements of Korean polymer research, and the demand for a multi-purpose beamline equipped with scattering and diffraction apparatus, the 4C2 bending magnet BL was constructed in 1997; it was upgraded to increase its output flux in 2000. The 4C2 BL is designed for various types of WAXS and SAXS experiments in the energy range 4-16 keV. The initial configuration of the 4C2 BL contained a 1:1 optical focusing configuration, in which its main optical component consisted of a bendable pre-mirror and a Si(111) double crystal monochromator. The pre-mirror, the monochromator, and the detector were located 16, 18, and 36 m from the source, respectively. The bendable pre-mirror focused the beam in a vertical direction and the second crystal of the monochromator was sagittally bent to focus the beam in the horizontal direction. The principal purpose of the upgrade was to install a toroidal focusing mirror to take over the role of the sagittal bending of the second crystal of the monochromator. The pre-mirror could then be used to collimate the beam and the second crystal of the monochromator was replaced with a flat crystal; vertical and horizontal focusing could then be carried out with the toroidal mirror. The monochromator was replaced with one fabricated for the 7C Electrochemistry BL at the PAL as a back-up unit. The flat collimating mirror, monochromator, and toroidal focusing mirror are now located 17, 18, and 20 m from the source, respectively. The detector position is fixed at 12.5 m from the focusing mirror. The upgraded 4C2 BL currently has a 2:1 optical focusing configuration.

In this paper, we summarize the current status of the instrumentation of the 4C2 BL and report some X-ray scattering measurements carried out on standard samples and polymeric materials, which were conducted to test the performance of the beamline optics and its detector systems. In addition, we report some grazing incidence X-ray scattering (GIXS) measurements for some polymer thin films.

Radiation Source

Figure 1(a) shows a photograph of the exterior of the Pohang Accelerator Laboratory (PAL).[64] The Pohang Light Source (PLS) is a 2.5 GeV synchrotron radiation source. The construction of the PLS was completed in September,

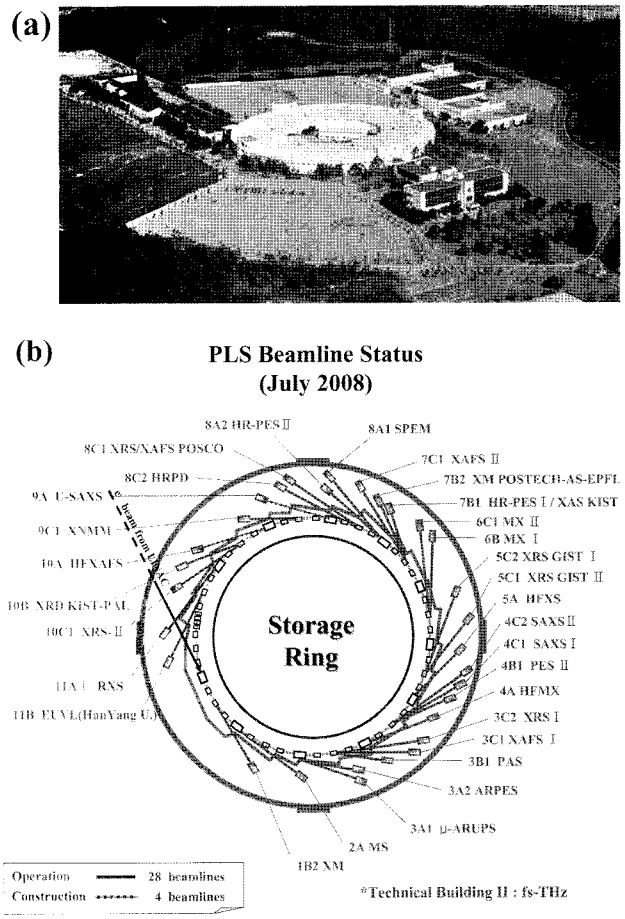

Figure 1. (a) Overhead view of the Pohang Accelerator Laboratory; (b) the status of the beamline at the Pohang Light Source.

1994. The PLS was designed to provide synchrotron radiation with continuous wavelengths down to 1 Å. The construction project was initiated in 1988. The PLS is a national facility that is owned and operated by the PAL and POSTECH on behalf of the Korean Government, and has been serving domestic and international users since September, 1995. The performance of the storage ring has been continuously improved since its construction. At the end of 2000, the PLS provided 430 mA at 2.0 GeV and 180 mA at 2.5 GeV. In response to user demand for more brilliant X-rays, the storage ring has been running at 2.5 GeV, 180 mA, since early 2000. There are a total of 32 beam ports, 22 from bending magnets and 10 from insertion devices. The maximum length available in a straight section for an insertion device is 4.3 m. 27 beamlines are currently in operation, with 4 further beamlines under construction including one in-vacuum undulator and one Wiggler insertion device beamline (Figure 1(b)).

The 4C2 BL is a bending magnet beamline with a magnetic field of 1.32 T. The dimensions of the source (root mean square deviation σ of the electron beam with respect

to the orbit) are σ_v=0.059 mm vertically and σ_h=0.160 mm horizontally, and the divergence of the emitted white beam is 0.1 mrad vertically and 3.0 mrad horizontally. At a stored electron energy of 2.5 GeV, the critical energy of radiation is 5.5 keV and a usable photon flux of up to 15 keV is delivered. The calculated angular photon flux density (which is specified in terms of the number of photons per unit time (s) per unit solid angle (mrad) per 0.1% relative bandwidth) is 2.15×10^{13} photons/s/mrad/0.1% band width at a stored electron energy of 2.5 GeV, a ring current of 200 mA, and an energy of radiation of 7.7 keV. The ultra-high vacuum in the storage ring is separated from the high vacuum beamline by a beryllium window.

Beamline Optics

Pre-mirror. A pre-mirror that consists of a single crystal of silicon with dimensions of 500 mm (L)×110 mm (W)× 60 mm (T) and that accepts a beam fan of 5 mrad is used to collimate the beam. The surface of the mirror was originally coated with Pt, but was recoated with Rh in the upgrade of the beamline. Rh has no absorption edge in the range 6-16 keV and a higher reflectivity than other materials such as Pt and Au. When the incidence angle of the mirror is 0.23°, the reflectivity for a 17 keV photon is below 40%. The mirror is dynamically bent with a torsional bender designed by the Exxon group for their beamlines at NSLS (National Synchrotron Light Source, Brookhaven, USA). The bending radius is about 4 km and is controlled with stepping motors. The mirror is cooled with water to dissipate the thermal load from the synchrotron radiation, which is estimated to be 10 W. The mirror bender and its support are shown in Figure 2.

Double Crystal Monochromator. The current double crystal monochromator (DCM) was originally designed and fabricated to back up the 7C electrochemistry beamline at the Pohang Light Source. The previous monochromator operated in the range 6-16 keV using Si(111) crystals; the second crystal was sagittally bendable for horizontal focusing. The back-up monochromator for the 7C electrochemistry beamline was found to be suitable for the 4C2 beamline with the addition of a focusing mirror. This monochromator is further modified compared to that of the 7C beamline. The whole system is housed in a 16.5 inch CF flange based chamber with a diameter of 350 mm and a height of 250 mm. A HUBER goniometer (model 420) is mounted on the flange outside the vacuum for the rotation of the crystals, and is used with a five phase stepping motor and a 100:1 harmonic drive, to produce an angular resolution of 1/100,000 degrees. Inside the flange, a rotational block is connected to the goniometer through a rotary feedthrough with a ferromagnetic seal. The first crystal is mounted on this block and its surface coincides with the rotational axis. The second crystal is mounted on a linear guide that is attached to the rotational block, and is translated along the normal to its surface to produce a fixed exit offset. There is no translation of the second crystal along its surface, because it is sufficiently long to allow for motion of the beam footprint. In addition, the second crystal is attached to two pico-motors for fine tuning of pitch and roll. There are three linear variable differential transformers, two for monitoring pitch and roll, and one for monitoring the distance between the crystals.

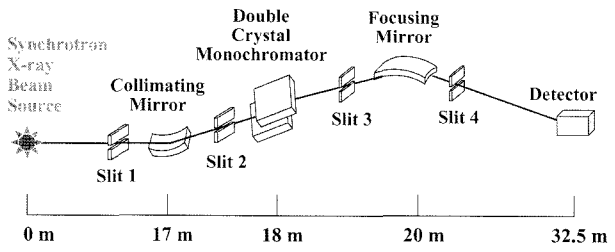

Figure 2. Schematic diagram of the SAXS 4C2 beamline at the Pohang Accelerator Laboratory.

Energy calibration is performed with the *K*-absorption edge of copper foil. Figure 3 shows the absorption spectrum of copper foil. This spectrum was measured with an ion chamber. As can be seen in Figure 3, the beamline was operated at an energy of 9.03 keV, which corresponds to a wavelength of 0.138 nm.

Focusing Mirror. In the new optical system, a toroidal focusing mirror is used in the main component with the double crystal monochromator discussed above. A flat pre-mirror is used for collimating rather than for vertical focusing as in the original configuration, and the second crystal in the new monochromator is not used for sagittal bending. Instead, the toroidal focusing mirror is used to carry out vertical and horizontal focusing. All the components of the manipulation system and the chamber other than the mirror bender were fabricated in the PAL. The specifications of the focusing mirror are shown in Table I.

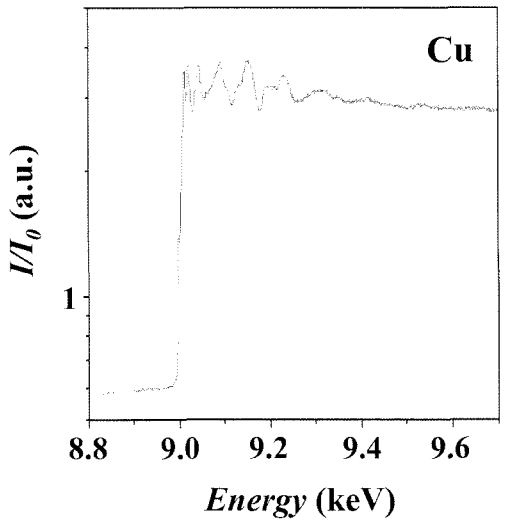

Figure 3. EXAFS *K*-edge spectrum of Cu foil measured with an ion chamber.

Table I. Specification for the SAXS Bendable Focusing Mirror

Shape	Bendable cylinder
Base material	Si monocrystal
Cylinder radius	5.3523 ± 0.05 cm
Coating	Rh 40 ± 5 nm + binder layer
Bending radius	4982.255 m(nominal)
Bendable range	∞ ~ 2500 m
Dimension	40(W) mm × 800(L) mm optical size
Surface roughness	5 Å
Slope error	< 1 arc sec in tangential direction < 5 arc sec in sagittal direction

Commissioning. As soon as the PTL construction was finished, simple measurements were performed to check the photon flux with a photodiode. We measured the output currents of other operating beamlines with a similar structure, and found that the output current of the 4C2 BL is as good as that of other beamlines. When the X-ray energy is 8 keV and the storage ring current is 160 mA, an output current from the Si photo-diode of 14 μA was observed, which corresponds to 3×10^{10} photons/sec/mrad/0.1% and is near the designed value. In addition, an EXAFS experiment was conducted to determine the energy resolution. Figure 3 shows the absorption spectrum of Cu foil. These results show that the collimating mirror and DCM function satisfactorily.

Detector

The SAXS camera is enclosed in a safety hutch and all components are remotely controlled. A motorized sample stage that provides flexibility in the positioning of the sample cells is located 22.5 m from the source. The photon flux at the sample position is estimated from the current measured with an ionization chamber to be approximately 2×10^{10} photons/mm^2/s at a ring current of 200 mA. Attenuators with various thicknesses can be inserted into the beam in order to control the photon flux on the sample. An evacuated beam path with adjustable length (10, 90, 130, or 170 cm) is mounted on a double optical rail between the sample and the detector stage. It is sealed at both ends with thin Kapton foils, and the vacuum level (typically 5×10^{-3} Torr) is continuously monitored. The beamstop is made of tantalum and is located inside the vacuum path at the end close to the Kapton window. A motor-controlled detector stage is installed right behind the vacuum path. The intensity of the primary beam can be monitored with ionization chambers in front of and/or behind the sample, and also with a scintillation counter that measures the back-scattering from the beamstop below an angle of approximately 45°.

Detector Systems

Charge-Coupled Device (CCD) Area Detector. An unintensified CCD area detector system (Roper Scientific, USA) was adopted as the SAXS detector and installed in February, 2003. The detector is based on a scientific grade full-frame array with multi-pinned-phase where charges are stored in an array of photosensitive capacitors. The beryllium entrance window of the detector has a diameter of 165 mm. Incident X-rays are converted by a GdOs phosphor screen into visible scintillation photons that are guided to the CCD image sensor by a demagnifying fiber optic taper with a reduction ratio of 2.4 : 1. The pixel size is 57.6×57.6 μm^2 at the entrance window and 24×24 μm^2 at the CCD image sensor. The sensor has a size of 50×50 mm^2 and is divided into 2084×2084 pixels. In order to reduce its dark current, the CCD is cooled to -50 °C with Peltier devices in combination with a circulating coolant. Water condensation inside the detector is prevented by evacuation. The output from the CCD is amplified, digitized with a 16-bit A/D converter, and transferred to the image memory of a Pentium computer via a high speed serial interface. The normal readout speed of the CCD at lowest noise is 100 kHz. The option of high speed readout at 1 MHz with a dynamic range of 16 bits per pixel is also available. The other methods for achieving a faster readout are the binning of pixels, partial readout, and a frame transfer mode. To prevent the smearing of the image during readout, an electromagnetic fast shutter that is triggered by the detector controller was installed in front of the sample. The detector is controlled using software provided by Roper Scientific (WinView32), which automates data acquisition, display, and basic processing. Further data processing such as circular averaging, scaling, background subtraction, and model fitting is carried out with other software that we have developed.

When the scattered beam arrives at the CCD detector, the precise measurement and subtraction of the dark charge signal is essential for an accurate determination of the low intensity pattern. The intensity of the dark signal from the CCD is low and exhibits little fluctuation over the array. Fluctuations are further reduced with circular averaging. There is a very small increase in the dark current at the CCD detector with integration time, which makes it possible to carry out measurements for samples with a low scattering intensity such as solutions. According to the manufacturer, the response nonuniformity is less than 2% over the entire CCD area. The good linearity of the detector within the dynamic range was reconfirmed. The operation of the detector was checked for the possible effects of spatial distortion of the fiber optic taper. For that purpose, the detector was illuminated through a brass grid patterned mask that consists of an array of holes 5 mm apart with a hole diameter of 0.25 mm. Figure 4 shows the image of the grid mask obtained with the CCD detector. The measured pattern of

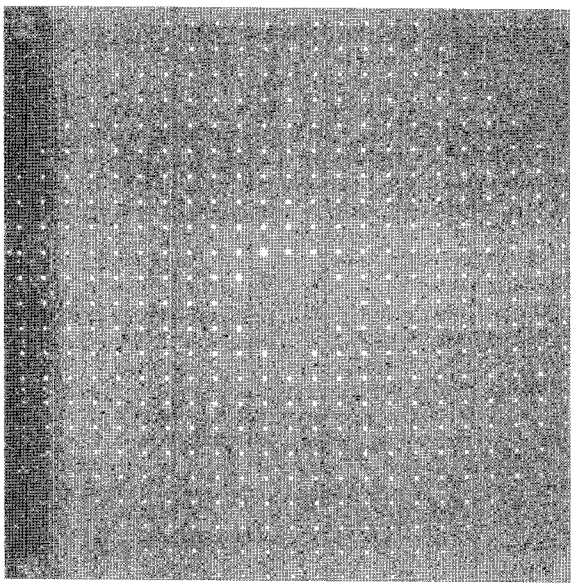

Figure 4. Image of a grid patterned mask obtained with the CCD detector.

the grid mask was compared with the real geometry of the grid, and found to provide a fairly good reproduction of the grid.

Experimental Results

Transmission X-ray Scattering Set-up.

Aqueous Polymer Dispersion: We now discuss the experimental data obtained for a polymer latex with the beamline. An aqueous suspension of a highly uniform, spherical poly(methyl methacrylate) (PMMA) latex was tested at a concentration of 17 vol%. To determine the intensity of scattering from the latex particles, we measured the scattering from water and from the empty sample cell and subtracted those contributions from the gross scattering curve for the aqueous dispersion, taking into account the respective transmission factors.[74] Figure 5 shows the SAXS results for the PMMA latex obtained with PLS 4C2 and with the ESRF (European Synchrotron Radiation Facility, Grenoble, France) undulator SAXS beamline ID2. The exposure times of the data obtained at ID2 and 4C2 are 0.1 s and 60 s respectively. The 4C2 scattering curve obtained with the CCD detector is in good agreement with the SAXS data for the same sample obtained at the ESRF.[75] The intensity is displayed on a logarithmic scale for better visualization of the data over the whole intensity range. Several oscillations of high and low intensity can be seen due to the form factor of these uniform, spherical particles. We found that the scattering intensity of this sample is so high that the contribution of any parasitic scattering to the measured intensity is negligible at all angles. Furthermore, the SAXS pattern shows that the accessible small angle region of the 4C2 BL is q=0.08 nm^{-1} (here, q is the scattering vector magnitude defined by $q=(4\pi/\lambda)\sin\theta$ where λ is the wavelength of the X-ray source and 2θ is the scattering angle), so measurements for a sample radius of less than 38.5 nm are possible. The collimation and energy resolution of the 4C2 beamline

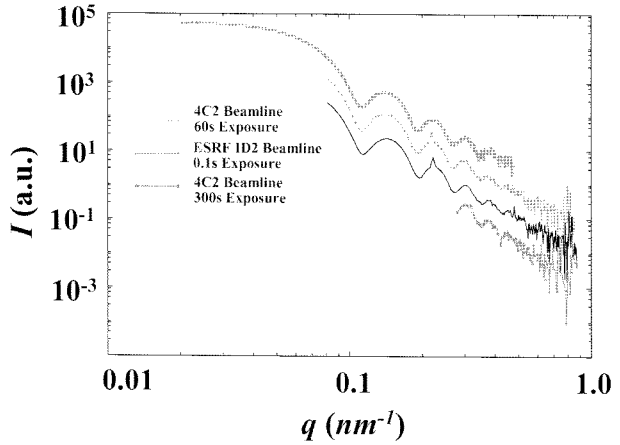

Figure 5. The circularly averaged SAXS profiles for a PMMA latex dispersion (approximately 17 vol%) obtained at the PLS 4C2 BL and the ESRF undulator SAXS beamline ID2. The exposure times of the data obtained at 4C2 and ID2 are 60 s and 0.1 s, respectively. The strong fluctuations of the CCD data at higher angles are mainly due to the large contributions of the dark signal and readout noise at the detector, which have to be subtracted.

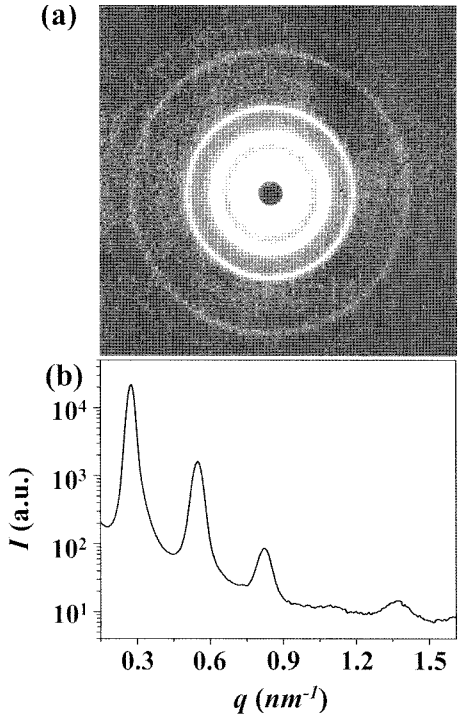

Figure 6. (a) Scattering pattern for a SEBS sample obtained with a CCD detector for an exposure time of 3 s. (b) Circularly averaged scattering profile extracted from (a). The plot is displayed on a logarithmic intensity scale in order to visualize the weaker diffraction peaks more clearly.

are adequate for measurements of samples with a 9% size distribution.

Block Copolymer: Figure 6(a) shows the scattering pattern obtained for a styrene-(ethylene-*co*-butylene)-styrene triblock copolymer (SEBS) by using a CCD detector system with an exposure time of 3 s. Several isotropic scattering rings (Debye-Scherrer rings) can be seen, which are due to the lamellar structure of SEBS. Figure 6(b) shows the circularly averaged scattering pattern extracted from the 2D pattern in Figure 6(a). As can be seen in this figure, there are several reflections with periodic spacing with relative scattering vector lengths from the specular reflection position of 1, 2, 3, 4, and 5. These scattering spots are characteristic of a lamellar structure, indicating that the phase-separated microdomains of SEBS form a lamellar structure within the sample. The long period of the lamellar structure was determined to be 23.02 nm.

Silver Behenate Powder: By decreasing the sample-to-detector distance to approximately 150 mm, wide-angle X-ray diffraction (WAXD) can be performed. Figure 7(a) shows the wide angle diffraction image obtained from a sample of silver behenate ($AgC_{22}H_{43}O_2$) powder by using the CCD detector with a exposure time of 5 s and a sample-to-detector distance of 162 mm. As can be seen in the image in Figure 7(a), there are a large number of reflections with regular spacing, which arise due to the periodic arrangement of the silver behenate molecules. Figure 7(b) shows the circularly averaged diffraction pattern extracted from the 2D pattern in Figure 7(a). The repeat distance, which was obtained by using benzoic acid as a cross-calibrated sample, was determined to be 5.838 nm. To calculate the repeat distance, a correction was applied to account for the distortion of the data that is due to the oblique incidence of the scattered beam onto the flat CCD detector; the solid angle subtended by one pixel on the detector changes with the scattering angle.[2] As can be seen in the inset in Figure 7(b), the position of each Bragg peak maximum is proportional to the order m of the peak. Thus silver behenate can be used for angle calibration and for the exact determination of the center coordinates of the incident beam.

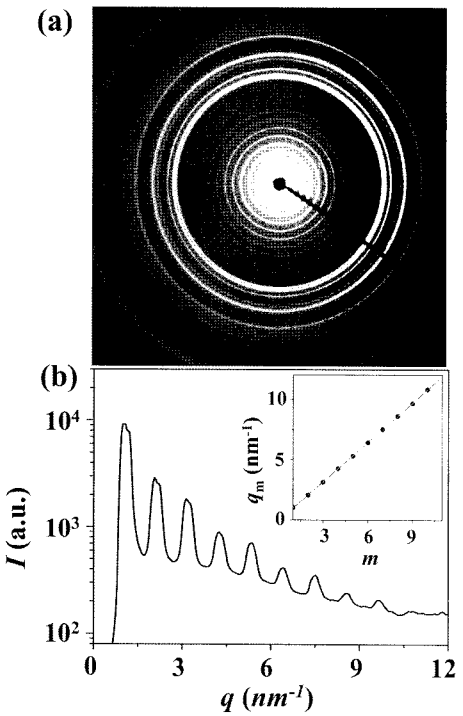

Figure 7. (a) Diffraction pattern from a silver behenate sample obtained with a CCD detector with an exposure time of 5 s. (b) Circularly averaged diffraction profile extracted from (a). The plot is displayed on a logarithmic intensity scale in order to visualize the weaker diffraction peaks more clearly. The inset shows the positions q_m of the Bragg peak maxima as a function of the order m of the peaks. The slope of the linear fit is inversely proportional to the d-spacing.

Grazing Incidence X-ray Scattering Set-up.

Grazing Incidence X-ray Scattering: Grazing incidence X-ray scattering (GIXS) has emerged as a very powerful technique for characterizing both the surface structures and internal structures of supported thin films.[54,55,58,59,76-97] As can be seen in Figure 8, the X-ray beam impinges at a grazing angle onto the sample slightly above the critical angle, so the film is fully penetrated by the X-ray beam. This technique offers several important advantages over transmission X-ray and neutron scattering: (i) a highly intense scattering pattern with high statistical significance is always obtained, even for films of nanoscale thickness, because the X-ray beam path length through the film plane is sufficiently long; (ii) there is no unfavorable scattering from the substrate on which the film is deposited; and (iii) easy sample preparation. For the GIXS measurements, a homemade z-axis goniometer equipped with a vacuum chamber was installed in the sample stage position. For

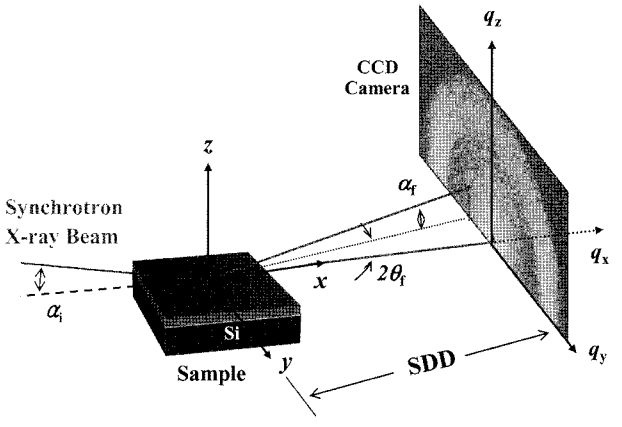

Figure 8. Geometry of GIXS: α_i is the incident angle at which the X-ray beam impinges on the film surface, α_f and $2\theta_f$ are the exit angles of the X-ray beam with respect to the film surface and to the plane of incidence, respectively, and q_x, q_y, and q_z are the components of the scattering vector **q**.

time-resolved measurements, the temperature of the sample stage can be controlled in the range -100 to 500 °C.

Cylindrical Nanoporous Thin Films: As an example of GIXS at the 4C2 beamline, measurements were obtained for cylindrical nanoporous thin films of two different thicknesses (28.5 and 78.8 nm) using the CCD detector. The cylindrical nanoporous thin films were prepared from vertically oriented nanodomain cylinders in 20-100 nm thick films supported on substrates, which consisted of a mixture of poly(styrene-*b*-methyl methacrylate) (PS-*b*-PMMA) and PMMA homopolymer.[84] The PMMA nanodomain cylinders were selectively etched out by ultraviolet light exposure and a subsequent rinse with acetic acid, resulting in a well-ordered nanostructure consisting of hexagonally packed cylindrical nanopores. The measurements were carried out with a sample-to-detector distance of 2,152 mm and an incidence angle of 0.2°, which is between the critical angle of the films and the silicon substrates. Aluminum foil strips were employed as semi-transparent beam stops because the intensity of the specular reflection from the substrate is much stronger than the intensity of GIXS near the critical angle. Data were collected for 1 s.

As can be seen in Figures 9(a) and (b), the GIXS patterns contain seven clear diffraction spots along the $2\theta_f$ direction (i.e., the in-plane direction) with relative scattering vector lengths from the specular reflection position of 1, $\sqrt{3}$, $\sqrt{4}$, $\sqrt{7}$, $\sqrt{9}$, $\sqrt{12}$, and $\sqrt{13}$. These diffraction spots are characteristic of a hexagonal structure, indicating that the nanopores generated by the removal of the PMMA microdomains are packed hexagonally in the film plane. The out-of-plane scattering profiles consist mainly of oscillations. These profiles resemble the specular X-ray reflectivity profiles of thin films that are modulated by Kiessig fringes. These fringes generally appear due to interference between the X-ray beams reflected from the film surface and those reflected from the film/substrate interface, namely the standing waves of the X-ray beam within the thin film. The film thickness can be estimated from the periodicity of the Kiessig fringes. The amplitude of Kiessig fringes is often modulated at a lower frequency if there is layer structure within the film. Furthermore, there is no feature characteristic of hexagonally packed nanopores in the out-of-plane scattering profiles, whereas such features are present in the in-plane scattering profiles. These results indicate that the nanopores in the films are preferentially oriented perpendicular to the film plane and occupy the whole film thickness; in other words, the nanopores have cylindrical shapes and heights comparable to the film thickness, and are oriented in the out-of-plane.

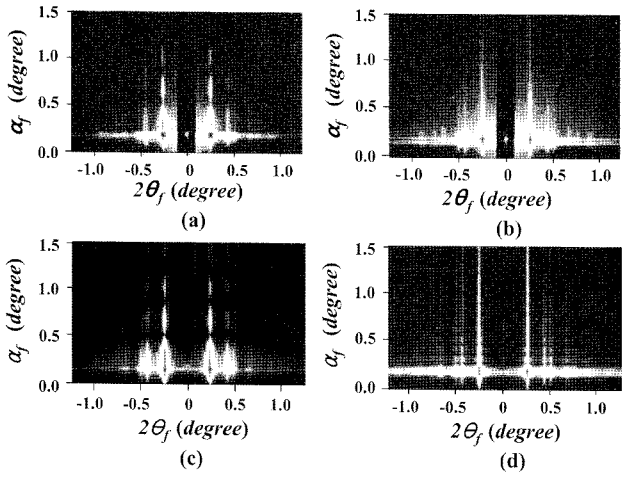

Figure 9. 2D GIXS patterns measured at α_i=0.20° for thin films of PS-*b*-PMMA/PMMA mixture deposited on silicon substrates after UV-etching: (a) 25.0 nm thick film; (b) 86.1 nm thick film. 2D GIXS patterns calculated for thin films of PS-*b*-PMMA/PMMA mixture deposited on silicon substrates after UV-etching: (c) 25.0 nm thick film; (d) 86.1 nm thick film.

To carry out a quantitative analysis, we derived the GIXS formula for hexagonal paracrystal lattices of cylinders.[84] The important structural parameters—cylinder shape, radius and radius distribution, length, center-to-center distance, orientation, degree of packing order, position distortion factor, electron density, and porosity—were then precisely determined from the scattering data. In addition, by using these structural parameters we calculated the 2D GIXS patterns using the GIXS formula. As can be seen in Figures 9(c) and (d), the calculated 2D GIXS patterns are in good agreement with the measured scattering patterns.

Gyroid Structures: Gyroid structures have received significant attention because of the interesting bicontinuous phase order often observed in various block copolymers and amphiphilic molecule systems. GIXS measurements were carried out at α_i=0.21° for thin films of polystyrene-*b*-polyisoprene (PS-*b*-PI) diblock copolymer, which were prepared on silicon substrates and then annealed at 160 °C for 1 day in vacuum.[77,80] The sample-to-detector distance was 2,500 mm and the incident angle α_i of the X-ray beam was set at 0.21°. A representative two-dimensional GIXS pattern is shown in Figure 10(a). This measured two-dimensional GIXS pattern contains a number of diffraction spots of a type commonly observed for gyroid structures, indicating that a gyroid structure is present in the block copolymer thin film. These diffraction spots are due to two different sets of diffractions originating from the reflected and transmitted X-ray beams, as reported previously.[77] The *d*-spacing of the first-order peak of the {121} plane was estimated to be 23.9 nm. Furthermore, the {121} plane of the gyroid structures in the film was found to be preferentially oriented parallel to the film plane. This experimental result was analyzed with the recently derived GIXS equation for gyroid structures with infinite periodic minimal surfaces, which are known to provide good approximations to gyroid structures.[91] The cubic lattice parameter a_G was found to be 58.7 nm and the mean width of PS phase L to be 14.5 nm

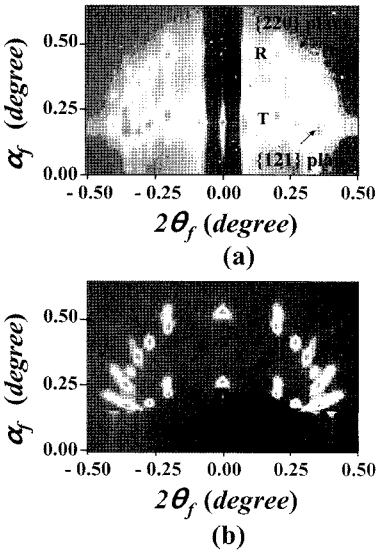

Figure 10. (a) 2D GIXS patterns measured at α_i=0.21° for a PS-*b*-PI thin film deposited on a silicon substrate and then annealed at 160 °C. **R** and **T** indicate the scattering spots generated by the reflected and transmitted X-ray beams respectively. (b) 2D GIXS patterns calculated with a recently derived GIXS equation for gyroid structures with infinite periodic minimal surfaces.

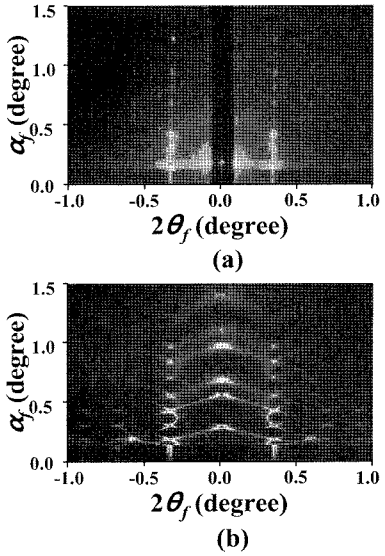

Figure 11. (a) 2D GIXS patterns measured at α_i=0.22° for a PS-*b*-PI thin film deposited on a silicon substrate and annealed at 120 °C. (b) 2D GIXS patterns calculated with a recently derived GIXS equation for hexagonally perforated layer structures.

with quantitative analysis. By using these structural parameters, we calculated the two-dimensional GIXS patterns using the GIXS formula with α_i=0.21°. A calculated two-dimensional GIXS pattern for a diblock copolymer film is shown in Figure 10(b), and is in good agreement with the measured scattering pattern, including reflections due to the reflected and transmitted X-ray beams, shown in Figure 10(b).

Hexagonally Perforated Layer Structure: Hexagonally perforated layer (HPL) structures are known to be metastable and appear in limited temperature ranges between the stable lamellar and gyroid phases, but have received much attention because of their intriguing structural characteristics such as the stacking sequence of the perforations modeled as ABC or AB arrangements or as a combination of ABC and AB. ABC stacking has rhombohedral symmetry ($R\bar{3}m$), whereas AB stacking has hexagonal symmetry ($p6_3/mmc$). GIXS measurements were carried out to quantitatively analyze the HPL structure of polystyrene-*b*-polyisoprene (PS-*b*-PI) diblock copolymer thin films supported on silicon substrates, which were annealed at 120 °C for 1 day.[77,80] The sample-to-detector distance was 2,300 mm and the incident angle α_i of the X-ray beam was set at 0.22°.

A representative 2D GIXS pattern for a HPL structure with an ABC stacking sequence is shown in Figure 11(a). As can be seen in this figure, the scattering pattern contains a number of sharp scattering spots over a wide range of scattering angles. In particular, the out-of-plane scattering spot arrays appear at relative $2\theta_f$ positions from the specular reflection position of 1, $\sqrt{3}$, $\sqrt{4}$, and $\sqrt{7}$. These observations indicate that a well-ordered in-plane hexagonal structure of microdomains is present in the film and that a certain lattice plane of the structure is aligned but randomly oriented in the film plane. These observations show that the *c*-axis of the hexagonal structure is oriented along a direction normal to the film plane, whereas the other two axes are randomly aligned in the film plane. These experimental results were analyzed with the recently derived GIXS equation for HPL structures with ABC stacking sequences, oriented cylindrical form factors, and rhombohedral symmetry.[93] The perforation distance a_H was found to be 30.6 nm and the repetitive thickness of ABC sequence to be 66.1 nm with quantitative analysis. By using these parameters and an ABC stacking sequence, the 2D GIXS pattern for the PS-*b*-PI diblock copolymer was calculated and is shown in Figure 11(b). GIXS and quantitative data analysis using the GIXS formula derived for HPL structures with ABC stacking were successfully applied to, and provided important structural details and properties for, PS-*b*-PI diblock copolymer thin films.

Lamellar Structure in the Side Chains of a Crystalline Polymer: The *n*-alkyl side chains of aliphatic polymers exhibit self-assembly behavior. We fabricated lamellar stack structures of poly(oxy(*n*-decylthiomethylenyl)ethylene) (PODTE) in thin films by spin-coating a solution of the brush polymer onto silicon substrates followed by drying, and then carried out synchrotron GIXS measurements. The measurements were performed at a sample-to-detector distance of 166 mm, and imaged using a 2D CCD.

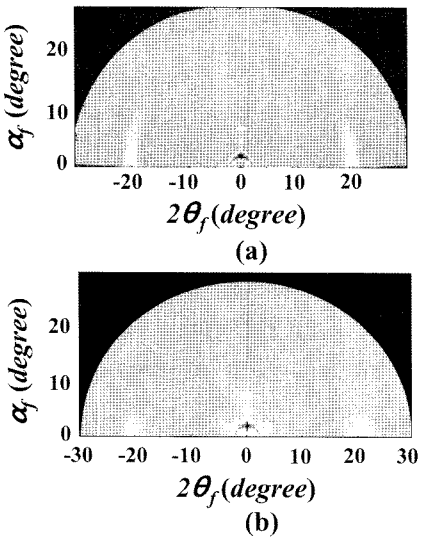

Figure 12. (a) 2D GIXS patterns measured at α_i=0.20° for a PODTE thin film deposited on a silicon substrate at -30 °C. (b) 2D GIXS patterns calculated with a recently derived GIXS equation for lamellar structures.

The measured 2D GIXS pattern for a PODTE thin film cooled to -30 °C, i.e., below its melting temperature T_m (=10.6 °C), is presented in Figure 12(a). Several strong scattering spots are present along the α_f direction at $2\theta_f$=0° (Figures 7(b) and 8(a)), with relative scattering vector lengths from the specular reflection positions of 1, 2, 3, and 4. Note that the first and third spots are more intense than the second and fourth spots. These scattering spots indicate the presence of a layered structure stacked normal to the film plane. In addition, there is one broad scattering arc along the $2\theta_f$ direction at α_f = 0°, with a peak maximum near $2\theta_f$ = 20° (Figure 12(a)), which is assigned to the inter-distance of the bristles in the PODTE polymer molecules. This experimental result was analyzed with the GIXS equation recently derived using paracrystal theory for lamellar structures with preferred orientations.[89] This analysis provided all the characteristics (long period, sub-layers and their thicknesses, volume fraction, bristle paracrystal distortion factor, and orientation) of the lamellar structure. Combining the determined structural parameters, including the orientation factor and positional disorder, we calculated the 2D GIXS patterns using the GIXS formula. A 2D GIXS pattern calculated for the film at -30 °C is presented in Figure 12(b). In this calculation, we assumed a contribution of 80% from the well-oriented, more ordered lamellar domains, and a contribution of 20% from the less-ordered lamellar domains with random orientation; the presences of the more-ordered lamellar domains as a major fraction and the less-ordered lamellar domains with random orientation as a minor fraction were confirmed with the above analysis of the measured 2D GIXS pattern. The calculated scattering patterns are in good agreement with the measured GIXS patterns shown in Figure 12(a). These results confirm that GIXS measurements can be carried out in the wide angle region at the 4C2 beamline.

Outlook

The energy resolution of the new optical system is significantly better than that of the original system. The output photon flux at the detector position is calculated, which is expressed with a dimension of photons/sec/mrad/0.1% band width. It is assumed that the opening of the slit is 1 mm and the acceptance angle in the horizontal direction is 1 mrad. In addition two Be windows with 250 μm thick, the Rh coated mirror with grazing angle and the collimating mirror with 10% slope error are considered in calculation of the photon flux. Here the slope error is a measure of surface ripple, i.e., long-range modulations or zones with wavelengths typically in the centimeter to tens-of-centimeters range.

In the SAXS experimental system, the sample stage and detector stage are separated so that the sample to detector distance can easily be adjusted. The detector stage position is fixed, but the sample stage can be moved along a guide rail. In addition, the separation of the sample stage and the detector stage has the advantage that a 4-circle kappa goniometer can be used instead of the sample stage for GIXS experiments. The 4C2 BL should be very useful to the polymer science and engineering community in Korea and elsewhere because of its stable and user-friendly beamline service.

Acknowledgment. This work was supported by the Ministry of Education, Science & Technology, POSCO, and the Korea Science and Engineering Foundation (National Research Lab for Polymer Synthesis and Physics and Center for Integrated Molecular Systems).

References

(1) A. Guinier and G. Fournet, *Small Angle Scattering of X-rays*, Chapman & Hall, London, 1955.
(2) O. Glatter and O. Kratky, Eds., *Small Angle X-ray Scattering*, Academic Press, London, 1982.
(3) L. A. Feigin and D. I. Svergun, *Structure Analysis by Small-Angle X-ray and Neutron Scattering*, Plenum Press, New York, 1987.
(4) H. Brumberger, Ed., *Modern Aspects of Small-Angle Scattering*, Kluver Academic Press, Dordrecht, 1995.
(5) R. J. Roe, *Methods of X-ray and Neutron Scattering in Polymer Science*, Oxford Univ. Press, Oxford, 2000.
(6) P. Cebe, B. S. Hsiao, and D. J. Lohse, Eds., *Scattering from Polymers: Characterization by X-rays, Neutrons and Light*, ACS Symposium Series 739, Oxford Univ. Press, 1999, and further references given therein.
(7) B. Chu and B. S. Hsiao, *Chem. Rev.*, **101**, 1727 (2001).

(8) S. Rojstaczer, M. Ree, D. Y. Yoon, and W. Volksen, *J. Polym. Sci. Part B: Polym. Phys.*, **30**, 133 (1992).
(9) M. Ree, T. L. Nunes, and J. S. Lin, *Polymer*, **35**, 1148 (1994).
(10) M. Ree, C. W. Chu, and M. J. Goldberg, *J. Appl. Phys.*, **75**, 1410 (1994).
(11) M. Ree, T. L. Nunes, and K. J. Chen, *J. Polym. Sci. Part B: Polym. Phys.*, **33**, 453 (1995).
(12) M. Ree, W. H. Goh, J. W. Park, M. H. Lee, and S. B. Rhee, *Polymer Bulletin*, **35**, 129 (1995).
(13) Y. Kim, M. Ree, T. Chang, and C. S. Ha, *Polymer Bulletin*, **34**, 175 (1995).
(14) M. Ree, W. H. Goh, and Y. Kim, *Polymer Bulletin*, **35**, 215 (1995).
(15) Y. Kim, M. Ree, T. Chang, C. S. Ha, T. L. Nunes, and J. S. Lin, *J. Polym. Sci. Part B: Polym. Phys.*, **33**, 2075 (1995).
(16) M. Ree, S. H. Woo, K. Kim, H. Chang, W. C. Zin, K.-B. Lee, and Y. J. Park, *Macromol. Symp.*, **118**, 213 (1997).
(17) M. Ree, K. Kim, S. H. Woo, and H. Chang, *J. Appl. Phys.*, **81**, 698 (1997).
(18) Y. Kim, W. K. Lee, W. J. Cho, C. S. Ha, M. Ree, and T. Chang, *Polym. Int.*, **43**, 129 (1997).
(19) J. K. Kim, H. H. Lee, M. Ree, K.-B. Lee, and J. Park, *Macromol. Chem. Phys.*, **199**, 641 (1998).
(20) S. M. Pyo, S. I. Kim, T. J. Shin, M. Ree, K. H. Park, and J. S. Kang, *Macromolecules*, **31**, 4777 (1998).
(21) S. M. Pyo, S. I. Kim, T. J. Shin, M. Ree, K. H. Park, and J. S. Kang, *Polymer*, **40**, 125 (1998).
(22) S. I. Kim, T. J. Shin, S. M. Pyo, J. M. Moon, and M. Ree, *Polymer*, **40**, 1603 (1999).
(23) S. I. Kim, T. J. Shin, and M. Ree, *Polymer*, **40**, 2263 (1999).
(24) S. M. Pyo, S. I. Kim, T. J. Shin, Y. H. Park, and M. Ree, *J. Polym. Sci. Part A: Polym. Chem.*, **37**, 937 (1999).
(25) S. I. Kim, T. J. Shin, M. Ree, G. T. Hwang, B. H. Kim, H. Han, and J. Seo, *J. Polym. Sci. Part A: Polym. Chem.*, **37**, 2013 (1999).
(26) M. Ree, T. J. Shin, T. L. Nunes, and W. Volksen, *Polymer*, **41**, 2105 (2000).
(27) Y.-K. See, J. Cha, T. Chang, and M. Ree, *Langmuir*, **16**, 2351 (2000).
(28) S. I. Kim, M. Ree, T. J. Shin, C. Lee, T.-H. Woo, and S. B. Rhee, *Polymer*, **41**, 5173 (2000).
(29) H. K. Park and M. Ree, *Synthetic Met.*, **117**, 197 (2001).
(30) I. S. Chung, C. E. Park, M. Ree, and S.Y. Kim, *Chem. Mater.*, **13**, 2801 (2001).
(31) J.-S. Kim, M. Ree, T. J. Shin, O. H. Han, S. J. Cho, Y.-T. Hwang, J. Y. Bae, J. M. Lee, R. Ryoo, and H. Kim, *J. Catal.*, **218**, 209 (2003).
(32) T. J. Shin, H. K. Park, S. W. Lee, B. Lee, W. Oh, J.-S. Kim, S. Baek, Y.-T. Hwang, H.-C. Kim, and M. Ree, *Polym. Eng. Sci.*, **46**, 1232 (2003).
(33) K. H. Choi, J. C. Jung, H. S. Kim, B. H. Sohn, W.-C. Zin, and M. Ree, *Polymer*, **45**, 1517 (2004).
(34) J.-S. Kim, H. Kim, J. Yoon, K. Heo, and M. Ree, *J. Polym. Sci. Part A: Polym. Chem.*, **43**, 4079 (2005).
(35) M. Ree, J. Yoon, and K. Heo, *J. Mater. Chem.*, **16**, 685 (2006).
(36) M. Ree, S. I. Kim, S. W. Lee, and J. H. Jung, *Polym. Sci. Technol. (Korea)*, **8**, 663 (1997).
(37) M. Ree, *Miscibility and Crystallization Behavior in Binary Polyethylene Blends*, in "Polyolefin Blends", D. Nwabunma and T. Kyu, Eds., Wiley, New York, 2007, Chapter 4.
(38) M. Ree, S. H. Woo, and T. J. Shin, *Polym. Sci. Technol. (Korea)*, **8**, 57 (1997).
(39) M. Ree, T. J. Shin, and S. W. Lee, *Korea Polym. J.*, **9**, 1 (2001).
(40) S. B. Lee, G. J. Shin, J. H. Chi, W. C. Zin, J. C. Jung, S. G. Hahm, M. Ree, and T. Chang, *Polymer*, **47**, 6606 (2006).
(41) Y. W. Chung, B. I. Lee, and B. K. Cho, *Macromol. Res.*, **16**, 113 (2008).
(42) Y. H. Shin, W. D. Lee, and S. S. Im, *Macromol. Res.*, **15**, 662 (2007).
(43) J. K. Choi, Y. W. Kim, J. H. Koh, J. H. Kim, and A. M. Mayes, *Macromol. Res.*, **15**, 553 (2007).
(44) U. Jeng, C. H. Hsu, Y. S. Sun, Y. H. Lai, W. T. Chung, H. S. Sheu, H. Y. Lee, Y. F. Song, K. S. Liang, and T. L. Lin, *Macromol. Res.*, **13**, 506 (2005).
(45) H. H. Song, M. Ree, D. Q. Wu, B. Chu, M. Satkowski, R. Stein, and J. C. Phillips, *Macromolecules*, **23**, 2380 (1990).
(46) H. H. Song, D. Q. Wu, M. Ree, R. S. Stein, J. C. Phillips, A. LeGrand, and B. Chu, *Macromolecules*, **21**, 1180 (1988).
(47) B. Lee, T. J. Shin, S. W. Lee, J. W. Lee, and M. Ree, *Macromol. Symp.*, **190**, 173 (2002).
(48) B. Lee, T. J. Shin, S. W. Lee, J. Yoon, J. Kim, and M. Ree, *Macromolecules*, **37**, 4174 (2004).
(49) J.-S. Kim, H. Kim, and M. Ree, *Chem. Mater.*, **16**, 2981 (2004).
(50) K. Heo, J. Yoon, K. S. Jin, S. Jin, G. Kim, H. Sato, Y. Ozaki, M. M. Satkowski, I. Noda, and M. Ree, *J. Appl. Crystallogr.*, **40**, s594 (2007).
(51) K. Heo, J. Yoon, K. S. Jin, S. Jin, H. Sato, Y. Ozaki, M. M. Satkowski, I. Noda, and M. Ree, *J. Phys. Chem. B*, **112**, 4571 (2008).
(52) B. Lee, T. J. Shin, S. W. Lee, J. Yoon, J. Kim, H. S. Youn, K.-B. Lee, and M. Ree, *Polymer*, **44**, 2509 (2003).
(53) T. J. Shin, B. Lee, H. S. Youn, K.-B. Lee, and M. Ree, *Langmuir*, **17**, 7842 (2001).
(54) B. Lee, Y.-H. Park, Y.-T. Hwang, W. Oh, J. Yoon, and M. Ree, *Nature Materials*, **4**, 147 (2005).
(55) B. Lee, W. Oh, Y. Hwang, Y.-H. Park, J. Yoon, K. S. Jin, K. Heo, J. Kim, K.-W. Kim, and M. Ree, *Adv. Mater.*, **17**, 696 (2005).
(56) J. Bolze, M. Ree, H. S. Youn, S. H. Chu, and K. Char, *Langmuir*, **17**, 6683 (2001).
(57) Y. Hwang, K. Heo, C. H. Chang, M. K. Joo, and M. Ree, *Thin Solid Films*, **510**, 159 (2006).
(58) Y. Kim, S. Cook, S. M. Tuladhar, S. A. Choulis, J. Nelson, J. R. Durrant, D. D. C. Bradley, M. Giles, I. McCulloch, C.-S. Ha, and M. Ree, *Nature Materials*, **5**, 197 (2006).
(59) Y. Kim, J. Nelson, J. R. Durrant, D. D. C. Bradley, K. Heo, J. Park, H. Kim, I. McCulloch, M. Heeney, M. Ree, and C.-S. Ha, *Soft Matter*, **3**, 117 (2007).
(60) W. Oh, Y. Hwang, T. J. Shin, B. Lee, J.-S. Kim, J. Yoon, S. Brennan, A. Mehta, and M. Ree, *J. Appl. Crystallogr.*, **40**, s626 (2007).
(61) G.-W. Lee, J. Kim, J. Yoon, J.-S. Bae, B. C. Shin, I. S. Kim, W. Oh, and M. Ree, *Thin Solid Films*, **516**, 5781 (2008).
(62) G.-W. Lee, K. S. Jin, J. Kim, J.-S. Bae, J. H. Yeum, M. Ree, and W. Oh, *Appl. Phys. A*, **91**, 657 (2008).

(63) W. Oh, Y. D. Park, Y. Hwang, and M. Ree, *Bull. Korean Chem. Soc.*, **28**, 2481 (2007).
(64) J. Bolze, J. Kim, J.-Y. Huang, S. Rah, H. S. Youn, B. Lee, T. J. Shin, and M. Ree, *Macromol. Res.*, **10**, 2 (2002).
(65) M. Ree and I. S. Ko, *Phys. High Tech. (Korea)*, **14**, 2 (2005).
(66) C.-J. Yu, J. Kim, K.-W. Kim, G.-H. Kim, H.-S. Lee, M. Ree, and K.-J. Kim, *J. Korean Vac. Soc.*, **14**, 138 (2005).
(67) D. S. Jang, H. J. Lee, B. Lee, B. H. Hong, H. J. Cha, J. Yoon, K. Lim, Y. J. Yoon, J. Kim, M. Ree, H. C. Lee, and K. Y. Choi, *FEBS Lett.*, **580**, 4166 (2006).
(68) J. M. Choi, S. Y. Kang, W. J. Bae, K. S. Jin, M. Ree, and Y. Cho, *J. Biol. Chem.*, **282**, 9941 (2007).
(69) D. Y. Kim, K. S. Jin, E. Kwon, M. Ree, and K. K. Kim, *Proc. Natl. Acad. Sci. USA*, **104**, 8779 (2007).
(70) J. H. Lee, G. B. Kang, H.-H. Lim, K. S. Jin, S.-H. Kim, M. Ree, C.-S. Park, S.-J. Kim, and S. H. Eom, *J. Mol. Biol.*, **376**, 308 (2008).
(71) K. S. Jin, D. Y. Kim, Y. Rho, V. B. Le, E. Kwon, K. K. Kim, and and M. Ree, *J. Synchrotron Rad.*, **15**, 219 (2008).
(72) S. Jin, T. Higashihara, T. Watanabe, K. S. Jin, J. Yoon, K. Heo, J. Kim, K.-W. Kim, A. Hirao, and M. Ree, *Macromol. Res.* (in press).
(73) K. S. Jin, J. K. Park, J. Yoon, Y. Rho, J.-H. Kim, E. E. Kim, and M. Ree, *J. Phys. Chem. B* (in press).
(74) N. Dingenouts, J. Bolze, D. Pötschke, and M. Ballauff, *Adv. Polym. Sci.*, **144**, 1 (1999).
(75) N. Dingenouts, *Röntgenkleinwinkelstreuung als Methodik der Strukturanalyse Teilgeordneter Systeme*, Shaker Verlag, Aachen, 1999.
(76) B. Lee, J. Yoon, W. Oh, Y. Hwang, K. Heo, K. S. Jin, J. Kim, K.-W. Kim, and M. Ree, *Macromolecules*, **38**, 3395 (2005).
(77) B. Lee, I. Park, J. Yoon, S. Park, J. Kim, K.-W. Kim, T. Chang, and M. Ree, *Macromolecules*, **38**, 4311 (2005).
(78) J.-S. Kim, H.-C. Kim, B. Lee, and M. Ree, *Polymer*, **46**, 7394 (2005).
(79) B. Lee, W. Oh, J. Yoon, Y. Hwang, J. Kim, B. G. Landes, J. P. Quintana, and M. Ree, *Macromolecules*, **38**, 8991 (2005).
(80) I. Park, B. Lee, J. Ryu, K. Im, J. Yoon, M. Ree, and T. Chang, *Macromolecules*, **38**, 10532 (2005).
(81) K. Heo, J. Yoon, and M. Ree, *IEE Proc. Bionanotechnology*, **153**, 121 (2006).
(82) J. Yoon, K. Heo, W. Oh, K. S. Jin, S. Jin, J. Kim, K.-W. Kim, T. Chang, and M. Ree, *Nanotechnology*, **17**, 3490 (2006).
(83) K. Heo, K. S. Jin, J. Yoon, S. Jin, W. Oh, and M. Ree, *J. Phys. Chem. B*, **110**, 15887 (2006).
(84) J. Yoon, S. Y. Yang, K. Heo, B. Lee, W. Joo, J. K. Kim, and M. Ree, *J. Appl. Crystallogr.*, **40**, 305 (2007).
(85) T. J. Lee, G.-S. Byun, K. S. Jin, K. Heo, G. Kim, S. Y. Kim, I. Cho, and M. Ree, *J. Appl. Crystallogr.*, **40**, s620 (2007).
(86) J. Yoon, S. C. Choi, S. Jin, K. S. Jin, K. Heo, and M. Ree, *J. Appl. Crystallogr.*, **40**, s669 (2007).
(87) K. S. Jin, K. Heo, W. Oh, J. Yoon, B. Lee, Y. Hwang, J.-S. Kim, Y.-H. Park, T. Chang, and M. Ree, *J. Appl. Crystallogr.*, **40**, s631 (2007).
(88) K. Heo, K. S. Oh, J. Yoon, K. S. Jin, S. Jin, C. K. Choi, and M. Ree, *J. Appl. Crystallogr.*, **40**, s614 (2007).
(89) J. Yoon, K. S. Jin, H. C. Kim, G. Kim, K. Heo, S. Jin, J. Kim, K.-W. Kim, and M. Ree, *J. Appl. Crystallogr.*, **40**, 476 (2007).
(90) K. Heo, S.-G. Park, J. Yoon, K. S. Jin, S. Jin, S.-W. Rhee, and M. Ree, *J. Phys. Chem. C*, **111**, 10848 (2007).
(91) S. Jin, J. Yoon, K. Heo, H.-W. Park, T. J. Shin, T. Chang, and M. Ree, *J. Appl. Crystallogr.*, **40**, 950 (2007).
(92) J. Yoon, S. W. Lee, S. Choi, K. Heo, K. S. Jin, S. Jin, G. Kim, J. Kim, K.-W. Kim, H. Kim, and M. Ree, *J. Phys. Chem. B*, **112**, 5338 (2008).
(93) K. Heo, J. Yoon, S. Jin, J. Kim, K.-W. Kim, T. J. Shin, B. Chung, T. Chang, and M. Ree, *J. Appl. Crystallogr.*, **41**, 281 (2008).
(94) S. Y. Yang, J. Park, J. Yoon, M. Ree, S. K. Jang, and J. K. Kim, *Adv. Funct. Mater.*, **18**, 1371 (2008).
(95) C.Yang, J. Yoon, S. H. Kim, K. Hong, K. Heo, M. Ree, and C. E. Park, *Appl. Phys. Lett.*, **92**, 243305 (2008).
(96) G. Kim, J. Yoon, J.-S. Kim, H. Kim, and M. Ree, *J. Phys. Chem. B* (in press).
(97) J. Yoon, S. Y. Jung, B. Ahn, K. Heo, S. Jin, T. Iyoda, H. Yoshida, and M. Ree, *J. Phys. Chem. B* (in press).